JOC Article

Hydrogen-Bond-Assisted Control of H versus J Aggregation Mode of Porphyrins Stacks in an Organogel System

Michihiro Shirakawa, Shin-ichiro Kawano, Norifumi Fujita, Kazuki Sada, and Seiji Shinkai*

Department of Chemistry and Biochemistry, Graduate School of Engineering, Kyushu University, 6-10-1 Hakozaki, Higashiku, Fukuoka 812-8581, Japan

seijitcm@mbox.nc.kyushu-u.ac.jp

Received February 10, 2003

To obtain insights into a correlation relationship between the structure and the aggregation mode in an organogel system, we synthesized gelators **2a**−**4a** bearing a porphyrin moiety as a one-dimensional aggregation unit and amide groups as peripheral hydrogen-bonding sites. Gelators **3a** and **3b** bearing the amide groups at the 4-position of the *meso*-phenyl groups are classified as versatile gelators, gelating 10 and 14 solvents, respectively, among 23 solvents tested herein. In contrast, gelators **2a** and **4a** bearing the amide groups at the 3,5-positions and 3-position, respectively, are classified as poor gelators. Examination by spectroscopic methods (UV−vis, ATR−FTIR, XRD, etc.) revealed that in the organogel phase porphyrins in **3a** adopt the H aggregation mode whereas those in **2a** and **4a** adopt the J aggregation mode. X-ray analysis of the single crystals established that in fact **3b** features a columnar stack of porphyrin moieties that can be classified as the H-aggregate, whereas **2a** results in a two-dimensional a−b plane, in which porphyrin moieties are arranged in the J-aggregate. Very interestingly, the difference in the H versus J aggregation mode is well-reflected by the difference in the macroscopic aggregate morphology observed by SEM: **3a** + cyclohexane gel results in a one-dimensionally aggregated fibrillar structure, whereas **2a** + cyclohexane gel results in a two-dimensional sheetlike structure. These findings indicate that the H versus J aggregation mode of porphyrin stacks can be controlled by the peripheral hydrogen-bonding interactions and the microscopic hydrogen-bonding network structure is well-reflected by the macroscopic SEM-observed structure.

Introduction

It is well-known that porphyrins and phthalocyanines tend to align into one-dimensional aggregates and therefore are of much concern in relation to creation of novel supramolecular architectures such as nanowires, discotic liquid crystals, helical ribbon structures, etc.[1−5] The major driving forces operating in these architectures are considered to be $\pi-\pi$ stacking and/or van der Waals interactions. More recently, another supramolecular architecture constructed in organogels has attracted broad attention of supramolecular chemists: the origin of organogel formation is considered to be one-dimensional alignment of gelator molecules supported by these interactions and/or hydrogen-bonding interactions.[6,7] This situation has offered a new idea that porphyrins and phthalocyanines, which a priori tend to assemble into one-dimensional supramolecular structures, would act as a powerful aggregative core for the design of new gelators. In addition, we have found that many new hydrogen-bond-based

(1) (a) van Nostrum, C. F.; Picken, S. J.; Schouten, A.-J.; Nolte, R. J. M. *J. Am. Chem. Soc.* **1995**, *117*, 9957−9965. (b) Schenning, A. P. H.; Benneker, F. B. G.; Geurts, H. P. M.; Liu, X. Y.; Nolte, R. J. M. *J. Am. Chem. Soc.* **1996**, *118*, 8549−8552. (c) van Nostrum, C. F.; Nolte, R. J. M. *Chem. Commun.* **1996**, 2385−2392. (d) Engelkamp, H.; van Nostrum, C. F.; Picken, S. J.; Nolte, R. J. M. *Chem. Commun.* **1998**, 979−980. (e) Engelkamp, H.; Middelbeek, S.; Nolte, R. J. M. *Science* **1999**, *284*, 785−788. (f) Samorí, S.; Engelkamp, H.; de Witte, P.; Rowan, A. E.; Nolte, R. J. M.; Rabe, J. P. *Angew. Chem., Int. Ed.* **2001**, *40*, 2348−2350 and references therein. (g) Tanaka, T.; Endo, K.; Aoyama, Y. *Bull. Chem. Soc. Jpn.* **2001**, *74*, 907−916.

(2) (a) Fuhrhop, J.-H.; Demoulin, C.; Boettcher, C.; Köning, J.; Siggel, U. *J. Am. Chem. Soc.* **1992**, *114*, 4159−4165. (b) Fuhrhop, J.-H.; Bindig, U.; Siggel, U. *J. Am. Chem. Soc.* **1993**, *115*, 11036−11037. (c) Bindig, U.; Schulz, A.; Fuhrhop, J.-H. *New J. Chem.* **1995**, *19*, 427−435 and references therein. (d) Bhyrappa, P.; Wilson, S. R.; Suslick, K. S. *J. Am. Chem. Soc.* **1997**, *119*, 8492−8502. (e) Patel, B. R.; Suslick, K. S. *J. Am. Chem. Soc.* **1998**, *120*, 11802−11803.

(3) (a) Smolenyak, P.; Peterson, R.; Nebesny, K.; Torker, M.; O'Brien, D. F.; Armstrong, N. R. *J. Am. Chem. Soc.* **1999**, *121*, 8628−8636. (b) Drager, S. A.; Zangmeister, R. A. P.; Armstrong, N. R.; O'Brien, D. F. *J. Am. Chem. Soc.* **2001**, *123*, 3595−3596.

(4) (a) Kimura, M.; Kitamura, T.; Muto, T.; Hanabusa, K.; Shirai, H.; Kobayashi, N. *Chem. Lett.* **2000**, 1088−1089. (b) Kimura, M.; Muto, T.; Takimoto, H.; Wada, K.; Ohta, K.; Hanabusa, K.; Shirai, H.; Kobayashi, N. *Langmuir* **2000**, *16*, 2078−2082. (c) Kimura, M.; Wada, K.; Ohta, K.; Hanabusa, K.; Shirai, H.; Kobayashi, N. *J. Am. Chem. Soc.* **2001**, *123*, 2438−2439.

(5) (a) Imada, T.; Murakami, H.; Shinkai, S. *Chem. Commun.* **1994**, 1557−1558. (b) Arimori, S.; Takeuchi, M.; Shinkai, S. *J. Am. Chem. Soc.* **1996**, *118*, 245−246. (c) Arimori, S.; Takeuchi, M.; Shinkai, S. *Supramol. Sci.* **1998**, *5*, 1−8.

(6) (a) Luboradzki, R.; Gronwald, O.; Ikeda, M.; Shinkai, S.; Reinhoudt, D. N. *Tetrahedron* **2000**, *56*, 9595−9599. (b) Hishikawa, Y.; Sada, K.; Watanabe, R.; Miyata, M. *Chem. Lett.* **1998**, 795−796. (c) Hachisako, H.; Ihara, H.; Kamiya, T.; Hirayama, C.; Yamada, K. *Chem. Commun.* **1997**, 19−20.

(7) For comprehensive reviews for organogels, see: (a) van Esch, J.; Schoonbeek, F.; de Loos, M.; Kooijman, H.; Veen, E. M.; Kellogg, R. M.; Feringa, B. L. In *Supramolecular Science: Where It Is and Where It Is Going*; Ungaro, R., Dalcanale, E., Eds.; Kluwar: The Netherlands, 1999; pp 233−259. (b) Melendez, R. E.; Carr, A. J.; Linton, B. R.; Hamilton, A. D. *Struct. Bond.* **2000**, 31−61. (c) Shinkai, S.; Murata, K. *J. Mater. Chem.* **1998**, *8*, 485−495.

10.1021/jo0341822 CCC: $25.00
Published on Web 05/08/2003

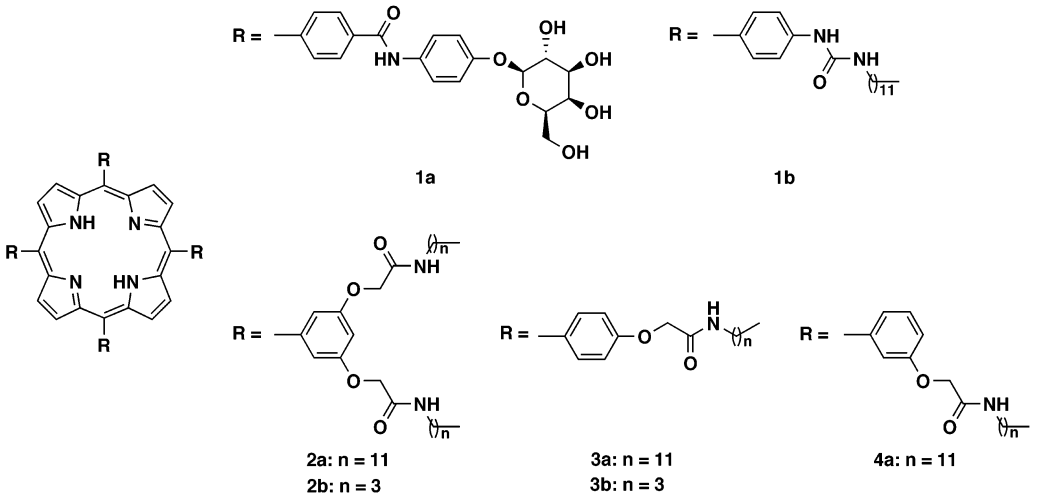

FIGURE 1. Molecular structures of **1a**, **1b**, **2a**, **2b**, **3a**, **3b**, and **4a**.

gelators can be developed utilizing a natural library of carbohydrate molecules.[8−10] These findings suggest that one-dimensional aggregates composed of porphyrins or phthalocyanines would be further "reinforced" by the hydrogen-bonding interaction among saccharide groups covalently appended to the central porphyrin (or phthalocyanine) column. However, this idea has scarcely been utilized for the design of a robust organogel system.[11] With these objects in mind we previously synthesized porphyrins **1a** and **1b** bearing four peripheral β-D-galactopyranoside groups and urea groups, respectively.[12] We found that **1a** results in stable organogels showing both thermotropic and lyotropic behaviors,[12a] whereas **1b** results in very stable organogels with values for T_{gel} (sol−gel phase transition temperature) higher than 140 °C. Further interestingly, the formed fibrous aggregate can be chirally twisted by addition of chiral urea derivatives.[12b]

In the course of these studies to extend **1a** to porphyrin-based gelators bearing a variety of peripheral saccharide groups, we noticed that some saccharides induce a blue shift of the Soret band, whereas other saccharides rather induce a red shift of the Soret band.[13] The finding implies that the hydrogen-bonding interactions among saccharide groups are able to finely tune the face-to-face orientation mode of porphyrin planes, resulting in the H-type or J-type aggregate in the organogel system. However, the hydrogen-bonding motifs constructed by saccharide groups are considerably complicated; in fact, it seems still difficult to establish a simplified correlation relationship between structure and aggregation mode from a library of saccharide-appended porphyrins. To obtain a clear insight into this relationship, we newly designed and synthesized gelators **2a**−**4a** bearing amide groups as a simplified hydrogen-bonding functional group (Figure 1). A series of **b** compounds was used as reference compounds for single-crystal X-ray analysis. Here, we report that the H versus J aggregation mode of porphyrins can be controlled by tailor-made molecular design utilizing the difference in the hydrogen-bonding array in the peripheral amide groups and each hydrogen-bonding motif found in the crystals is well-correlated with each macroscopic aggregate morphology observed by electron micrographs.

Results and Discussion

Gelation Test. The gelation properties have been tested for 23 different solvents. The gelation test was carried out as follows. The gelator was mixed in a capped test tube with the appropriate amount of solvent, and the mixture was heated until the solid was dissolved. By this procedure the solvent boiling point becomes higher than that under standard atmospheric pressure. The sample vial was cooled in air to 25 °C, left for 1 h at this temperature, and then turned upside down. When the gelator formed a clear or slightly opaque gel by immobilizing the solvent at this stage, it was denoted by a "G" mark in Table 1.

From the foregoing gelation test, one may conclude that **3a** and **3b** bearing the amide groups at the 4-position of the *meso*-phenyl groups are classified as versatile gelators, gelating 10 and 14 solvents, respectively, among 23 solvents tested herein. It was a big surprise to us that **3b**, which was synthesized as a reference compound of **3a** to prepare the single crystal, also acts as a versatile gelator. In contrast, **2a** and **4a** bearing the amide groups at the 3,5-positions and 3-position of the *meso*-phenyl groups, respectively, are classified as poor gelators.

(8) (a) Yoza, K.; Ono, Y.; Yoshihara, K.; Akao, T.; Shinmori, H.; Takeuchi, M.; Shinkai, S.; Reinhoudt, D. N. *Chem. Commun.* **1998**, 907−908. (b) Yoza, K.; Amanokura, N.; Ono, Y.; Akao, T.; Shinmori, H.; Shinkai, S.; Reinhoudt, D. N. *Chem. Eur. J.* **1999**, *5*, 2722−2729. (c) Amanokura, N.; Yoza, K.; Shinmori, H.; Shinkai, S.; Reinhoudt, D. N. *J. Chem. Soc., Perkin Trans. 2* **1998**, 2585−2591. (d) Gronwald, O.; Sakurai, K.; Luboradzki, R.; Kimura, T.; Shinkai, S. *Carbohydr. Res.* **2001**, *331*, 307−318.

(9) For a comprehensive review for sugar-based gelators, see: Gronwald, O.; Shinkai, S. *Chem. Eur. J.* **2001**, *7*, 4329−4334.

(10) Luboradzki, R.; Gronwald, O.; Ikeda, A.; Shinkai, S. *Chem. Lett.* **2000**, 1148−1149.

(11) Similar porphyrin derivatives were synthsized by Fuhrhop's group[2] but were not applied to the organogel system. More recently, Stoddart et al. synthesized sugar-coated discotic liquid crystals bearing a triphenylene core, but the gelation properties were not examined therein: Barbera, J.; Garces, A. C.; Jayaraman, N.; Omenat, A.; Serrano, J. L.; Stoddart, J. F. *Adv. Mater.* **2001**, *13*, 175−180.

(12) (a) Tamaru, S.-i.; Nakamura, M.; Takeuchi, M.; Shinkai, S. *Org. Lett.* **2001**, *3*, 3631−3634. (b) Tamaru, S.-i.; Uchino, S.-y.; Takeuchi, M.; Ikeda, M.; Hatano, T.; Shinkai, S. *Tetrahedron* **2002**, *43*, 3751−3755.

(13) Kawano, S.-i.; Tamaru, S.-i.; Fujita, N.; Shinkai, S. *Chem. Eur. J.* Submitted for publication.

TABLE 1. Organic Solvents Tested for Gelation with 2a, 3a, 4a, 2b, and 3b[a]

solvent	2a	3a	4a	2b	3b
benzene	P	P	S	G	G
toluene	P	P	S	G	G
p-xylene	G	P	S	P	G
pyridine	S	S	S	S	S
diphenyl ether	P	G	S	G	G
anisole	P	P	S	P	G
tetralin	G	S	S	P	G
cyclohexane	G^{++}	G^{++}	G^{--}	I	I
methylcyclohexane	G^{++}	G^{++}	G	I	P
hexane	P	P	P	I	I
octane	G^{++}	G^{++}	G^{-}	I	P
1-octanol	S	P	S	G	G
1-butanol	S	P	S	S	G
2-propanol	S	G	S	S	G
1-propanol	S	G^{+}	S	S	G
ethanol	S	G^{+}	S	S	G
methanol	P	G^{++}	P	S	P
acetonitrile	P	P	P	S	P
ethyl acetate	P	P	S	S	G
acetone	P	G^{+}	S	S	G
THF	S	S	S	S	S
dioxane	S	S	S	S	S
carbon tetrachloride	G	G	S	I	G

[a] G^{++}, G^{+}, G, G^{-}, and G^{--} denote stable gel formaton at 10.0, 12.5, 25.0, 30.0, and 50.0 g dm^{-3}, respectively. S, P, and I denote solution, precipitation, and insoluble, respectively.

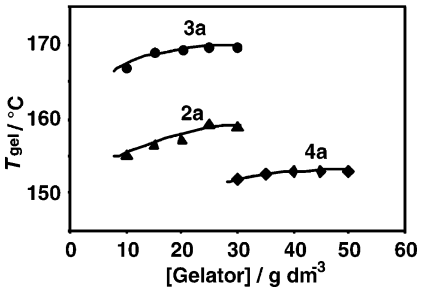

FIGURE 2. Plots of T_{gel} against gelator concentration in octane: (▲) **2a**, (●) **3a**, and (♦) **4a**.

To compare the thermal stability of **2a**, **3a**, and **4a** gels we determined their T_{gel} values in octane, which is commonly gelated by these three compounds (Figure 2). It is seen from Figure 2 that in a sealed test tube, all T_{gel} values are higher than the boiling point of octane (125.7 °C), and among them, the T_{gel} values appear in the order of **3a** > **2a** > **4a**. It is worthy of note that **3a** bearing four amide groups can result in a gel more stable than **2a** bearing eight amide groups. Careful examination of the gelation ability of **3a** and **3b** reveals that they gelate not only hydrocarbon solvents but also alcoholic solvents such as ethanol, 1-propanol, 2-propanol, etc. The hydrogen-bonding interaction can operate effectively in aprotic solvents but is considerably weakened in alcoholic solvents. Thus, the gelation of these solvents in protic solvents should be supported mainly by the van der Waals interaction among porphyrin planes. One may consider, therefore, that when the hydrogen-bonding interaction and the van der Waals interaction act cooperatively in a one-dimensional molecular stack, efficient gelation can take place. In the molecular design of porphyrin-based gelators, we expected that the porphyrin−porphyrin distance (4.8 Å as estimated from the X-ray crystallographic analysis) would be comparable with the distance of one hydrogen-bonded amide group.[14] This implies that if the 4-amide groups in **3a** or **3b** interact according to the intermolecular amide−amide hydrogen bonds into a direction parallel to a one-dimensional porphyrin stack, **3a** or **3b** should construct a "perfect" one-dimensional column consisting of cooperative amide−amide and porphyrin−porphyrin interactions. In **2a** or **2b** having two amide groups on one *meso*-phenyl group, on the other hand, one cannot expect the formation of such a one-dimensional column. Moreover, molecular modeling suggests that with the 3-amide groups in **4a** it is sterically difficult to construct a hydrogen-bonding array into a direction parallel to a one-dimensional porphyrin stack. This means that the aggregate structure of **2a**, **2b**, or **4a** must be different from that of **3a** or **3b**. The experimental issue that **3a** acts much better as a gelator than **2a** is, therefore, compatible with the molecular design principle in the initial working hypothesis. What is the origin of this disagreement? The decisive answer to this question was obtained from the following X-ray crystallographic analysis of the single crystals. Before that, however, we measured the UV−vis absorption spectra to obtain an insight into the aggregation mode of porphyrin moieties.

UV−vis Absorption Spectra. Spectroscopic discrimination between the H versus J porphyrin−porphyrin stacking mode is achieved by UV−vis absorption spectral examinations. In the Soret band, the blue shift is a sign of the H-aggregate formation whereas the red shift is a sign of the J-aggregate formation.[15] In the gel phase, the gelator concentrations were so high that the spectra could not be obtained using a conventional optical cell. Thus, the gel phase spectra were measured with a gel sample sandwiched by two glass plates, so that the ordinate is expressed with an arbitrary unit.

As shown in Figure 3b, the Soret band for **3a** appearing at 418.5 nm in the sol phase shifted to shorter wavelength down to 410.5 nm in the gel phase. In contrast, the Soret band for **2a** and **4a** appearing at 421.5 and 417.0 nm in the sol phase, respectively, shifted to longer wavelength up to 427.0 and 425.5 nm in the gel phase (Figure 3a and 3c). The contrasting λ_{max} shifts indicate that porphyrins in the **3a** gel are enforced to adopt the H aggregation mode whereas those in the **2a** and **4a** gels enjoy the conventional J aggregation mode. The results indicate that the difference in the hydrogen-bonding motif affects the porphyrin aggregation mode, which is reflected by the difference in the absorption spectra.

X-ray Crystallographic Analysis of Single Crystals. In general, gelator molecules tend to pile up in a one-dimensional direction and result in needlelike crystals. This growth mode makes it difficult to obtain a single crystal suitable for X-ray crystallographic analysis. As expected, growth of a single crystal from **2a** and **3a** resulted in failure. However, we succeeded in growth of single crystals from **2b** and **3b**, reference compounds bearing shorter aliphatic chains. Compounds **2b** and **3b**

(14) (a) Leiserowitz, L.; Tuval, M. *Acta Crystallogr.* **1978**, *B34*, 1230−1247. (b) Etter, M. C. *Acc. Chem. Res.* **1990**, *23*, 120−126.

(15) (a) Kano, K.; Fukada, K.; Wakami, H., Nishiyabu, R.; Pasternack, R. F. *J. Am. Chem. Soc.* **2000**, *122*, 7494−7502. (b) Král, V.; Schmidtchem, F. P.; Lang, K.; Berger, M. *Org. Lett.* **2002**, *1*, 51−54. (c) Maiti, N. C.; Mazumdar, M.; Periasamy, N. *J. Phys. Chem. B* **1998**, *102*, 1528−1538.

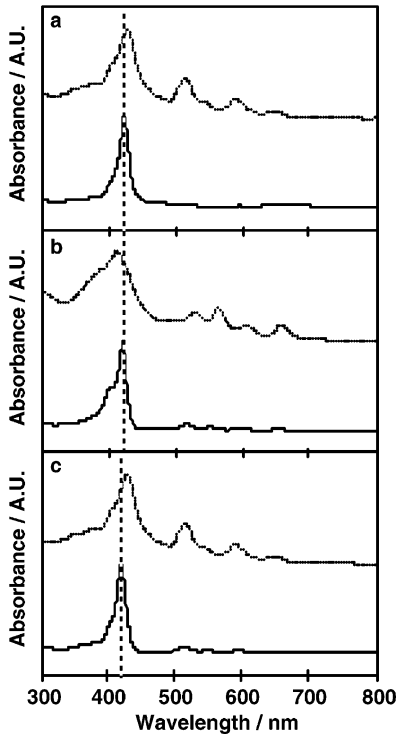

FIGURE 3. UV−vis absorption spectra in the sol phase (—) and the gel phase (· · ·): (a) **2a**, (b) **3a**, and (c) **4a**.

TABLE 2. Crystallographic Data of Compound 2b and 3b

	2b	**3b**
formula	$C_{92}H_{118}N_{12}O_{16}$	$C_{72}H_{74}N_8O_{10}$
formula weight	1648.99	1211.42
crystal system	triclinic	triclinic
space group	*P*-1 (No. 2)	*P*-1 (No. 2)
a (Å)	15.350 (4)	18.591 (2)
b (Å)	16.585 (4)	20.848 (2)
c (Å)	12.858 (4)	9.5842 (8)
α (deg)	107.35(1)	91.983(4)
β (deg)	104.190 (7)	101.562 (5)
γ (deg)	115.63(1)	93.631(2)
V (Å^3)	2536 (1)	3627.7 (6)
Z	2	2
D_c (g/cm^3)	1.211	1.109
μ (cm^{-1})	6.71	6.04
T (K)	123.2	123.2
no. of unique reflections	8205	11797
no. of observed reflections	4966	4118
R_1, R_w	0.12, 0.32	0.16, 0,38
GOF	1.90	1.98
2*θ*max (deg)	136.4	136.4
R/*P*	8.2	5.7
crystal habit	chunk	needle

were recrystallized from acetone−hexane and tetrahydrofuran−acetonitrile, respectively. Their crystal data are summarized in Table 2.

The crystal structure of **2a** is shown in Figure 4. The porphyrin rings are arranged two-dimensionally in an a−b plane to form a layer structure coplanar to the porphyrin rings, and the amide groups are used to connect them within the layer. One hydrogen-bonding network that runs parallel to the layer consists of four amide groups from four different porphyrins. As a result, the two terminal amide groups remain unpaired hydrogen-bond sites (arrow marks in Figure 4). The layer−layer distance along the *c*-axis is 12.858 Å, which is too far for porphyrins to enjoy *π*−*π* stacking interaction (Figure 5). Instead, the layer−layer space is filled with the alkyl groups of the amide groups and the solvated molecules. One can thus conclude that the crystal packing mode of porphyrin rings in **2b** has a two-dimensional character without the direct porphyrin−porphyrin interaction. That is because one *meso*-phenyl group has two amide groups at the 3- and 5-positions and the hydrogen-bonding force plays a decisive role to determine the structure.

The crystal structure obtained from **3b** was totally different from that obtained from **2a**. Porphyrin rings form a one-dimensional packing column, and the four columns are connected by hydrogen bonds among the amide groups to give a quadrilateral network manner. In the column, the porphyrin−porphyrin distance is 4.8 Å, which is comparable with that obtained from other porphyrin crystals.[16] As shown by space-filling models in Figure 7, porphyrin rings in one columnar structure really enjoy the *π*−*π* stacking interaction. One porphyrin in a column is connected with two porphyrins in the neighboring column, as shown in Figure 6 or 7. The infinite hydrogen-bonding network runs perpendicular to the porphyrin ring along the *π*-stack column. In total, all amide groups are used to construct the one-dimensional hydrogen-bonding array. One may regard, therefore, that in **3b** (and also in **3a**) the porphyrin−porphyrin stacking interaction and the amide−amide hydrogen-bonding interaction operate cooperatively to form a columnar superstructure.

Powder X-ray Diffraction. The XRD spectra of xerogels obtained from **2b** + benzene gel and **3b** + benzene gel are shown in Figures 8a and 9a, respectively. As the "theoretical" XRD spectra can be illustrated using the X-ray crystallographic data, they are shown in Figures 8b and 9b, respectively. In Figure 8b, one can recognize a strong peak at $2\theta = 6.87°$ ($d = 12.9$ Å), which is ascribed to the refraction from the (001) plane constructed by the porphyrin layers. The same peak is also observable in Figure 8a, indicating that the xerogel also has the (001) plane. Other "theoretical" peaks in Figure 9b are mostly found as "experimental" peaks in Figure 9a. On the other hand, Figure 9b shows two strong peaks at $2\theta = 4.24°$ and 4.75° ($d = 20.8$ and 18.6 Å), which are ascribed to the refraction from the (100) and (010) planes related to the distances between porphyrin columns. Again, these peaks also appear in Figure 9a and the spectral patterns are similar to each other between "theoretical" Figure 9b and "experimental" Figure 9a.

The foregoing findings support the view that in the present porphyrin-based organogel system, the packing mode of the molecular assemblies constructed in the organogels are very similar to those grown in the single crystals.

ATR-FTIR Spectral Analysis. The X-ray analysis results obtained from **2b** and **3b** have allowed us to predict that even in the gel phase the amide groups in **3a** and **3b** are totally used to form the hydrogen bonds (see Figure 6), whereas **2a** and **2b** have two free carbonyl

(16) (a) Byrn, M. P.; Curtis, C. J.; Goldberg, I.; Hsiou, Y.; Khan, S. I.; Sawin, P. A.; Tendick, S. K.; Strouse, C. E. *J. Am. Chem. Soc.* **1991**, *113*. 6549−6557. (b) Byrn, M. P.; Curtis, C. J.; Hsiou, Y.; Khan, S. I.; Sawin, P. A.; Tendick, S. K.; Terzis, A.; Strouse, C. E. *J. Am. Chem. Soc.* **1993**, *115*. 9480−9497.

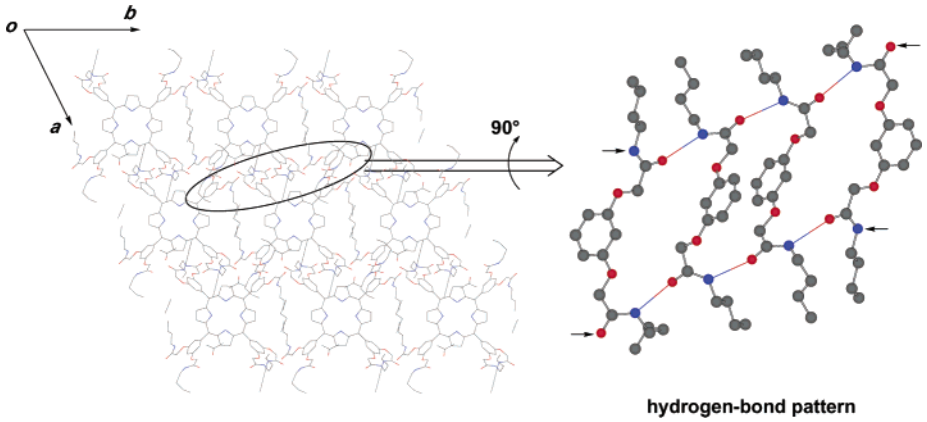

FIGURE 4. The hydrogen bond pattern in the crystal structure of **2b**. The arrows show the unsaturated hydrogen-bonding sites.

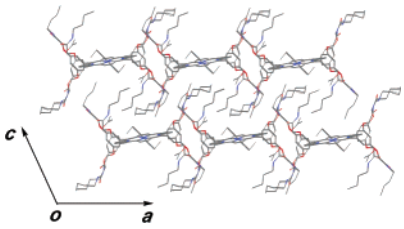

FIGURE 5. Side view of the two layers' packing obtained from crystal structure of **2b**.

and two free NH groups among eight amide groups (see Figure 4). Taking the molecular symmetry into account, one may presume that **4a** also employs a hydrogen-bonding mode similar to that of **2b**. To confirm these lines of conjecture, we prepared cyclohexane gels of **2a**, **3a**, and **4a** and benzene gels of **2b** and **3b** and subjected their xerogels to ATR−FTIR spectral analysis.

In general, the amide group represents two IR bands, amide I in the 1660 cm^{-1} region and amide II in the 1580 cm^{-1} region. As shown in Figure 10b, the xerogel obtained from **3b** + benzene gel gives two peaks at 1653 and 1545 cm^{-1}, which are assignable to these amide I and II bands, respectively. The IR spectrum of the xerogel obtained from **3a** + cyclohexane gel is basically very similar to that shown in Figure 3b. The results indicate that, as shown by the X-ray crystallographic studies, the amide groups in **3a** and **3b** are totally used for the formation of hydrogen bonds. On the other hand, the IR spectrum of the xerogel obtained from **2b** + benzene gel has two peaks for each amide region (Figure 10a). This split pattern is also observed for amide regions of **2a** + cyclohexane gel. This can be understood as a sign that the gels consist of both the hydrogen-bonded and the non-hydrogen-bonded amide groups. The xerogel obtained from **4a** + cyclohexane gel afforded several peaks at these amide regions, indicating that the hydrogen-bonding array is considerably disordered. The foregoing results are summarized in Table 3. Thus, the packing modes are classified, from the viewpoint of the hydrogen-bonding pattern, into three categories: fully hydrogen-bonded, partially hydrogen-bonded, and disordered. The difference is basically associated with the compatibility between one-dimensional porphyrin packing mode and amide−amide hydrogen-bonding mode. Further importance is the finding that the IR spectra of the xerogels are well-explained by the X-ray crystallographic data.

SEM Observation. The foregoing X-ray crystallographic and spectroscopic studies consistently suggest that **2a** should grow up to some two-dimensional aggregate, for example, as sheets, whereas **3a** should grow up to some one-dimensional aggregate, for example, as fibers. It is interesting to know whether these microscopic hydrogen-bonding patterns are really reflected by the macroscopic superstructures. Figure 11a shows a xerogel SEM image of **2a** + cyclohexane gel. It is clearly seen from this SEM picture that the gel consists of the sheetlike aggregates. As shown in Figure 11b, on the other hand, **3a** + cyclohexane gel results in a network structure consisting of fibrillar aggregates with ca. 50 nm diameter. One may conclude, therefore, that the microscopic packing modes identified by spectroscopic and X-ray crystallographic studies are rigorously reproduced in the macroscopic structures as detected by SEM.

Conclusion

The present study established that porphyrin acts as a potential central core to form a one-dimensional molecular stack for organogel fibers. Furthermore, it was shown that the stacking mode is finely tuned by the hydrogen-bonding interactions among peripheral amide groups, that is, both H and J aggregation structures are readily prepared by a slight change in the hydrogen-bonding motif. As a basic molecular design principle, the H-aggregate results when the column consists of one porphyrin−porphyrin pitch and one amide−amide pitch whereas the aggregates other than the H-aggregate results when this principle is not satisfied. This implies that also in porphyrin-based gelators with peripheral saccharide groups,[12,13] the compatibility between the porphyrin−porphyrin pitch and the hydrogen-bonded OH−OH pitches should play an important role to determine the aggregation structure. We now believe that this molecular design principles is useful not only to develop new robust porphyrin-based gelators but also to arrange porphyrins in various spatial positions in three-dimensional crystals. The porphyrin matrixes thus obtained are, expectedly, sensitively reflected by the functions of porphyrin moieties such as photochemical reactions, fluorescence properties, metal binding properties, etc.

Experimental Section

Measurement of Sol−Gel Transition Temperatures. The sealed tube containing the gel was immersed inversely

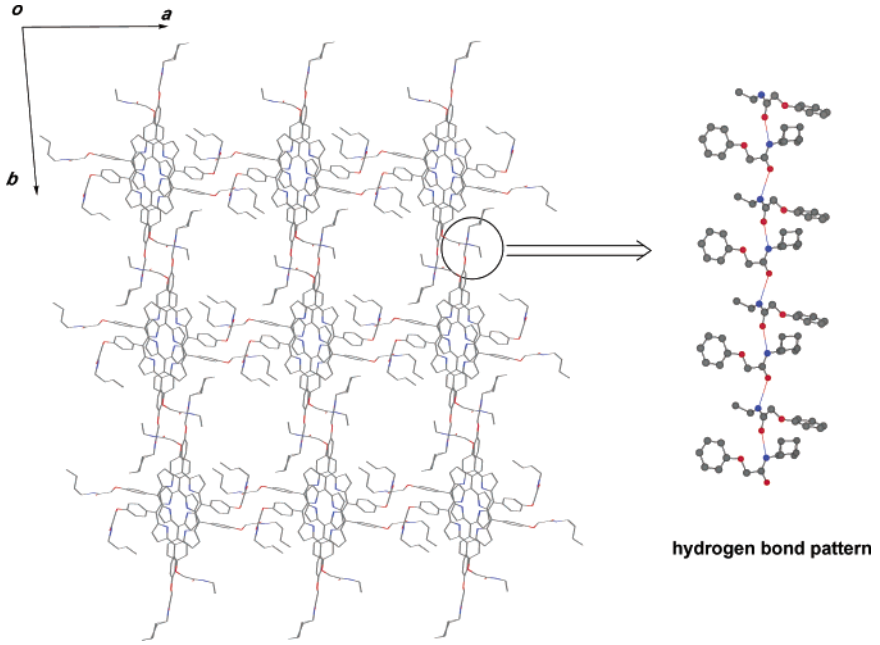

FIGURE 6. The hydrogen bond pattern in the crystal structure of **3b**.

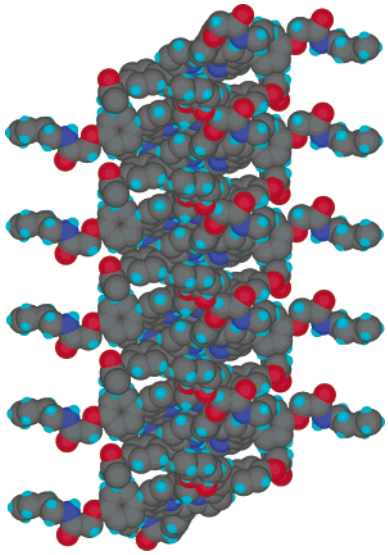

FIGURE 7. Side view of the one columnar structure obtained from the crystal structure of **3b**.

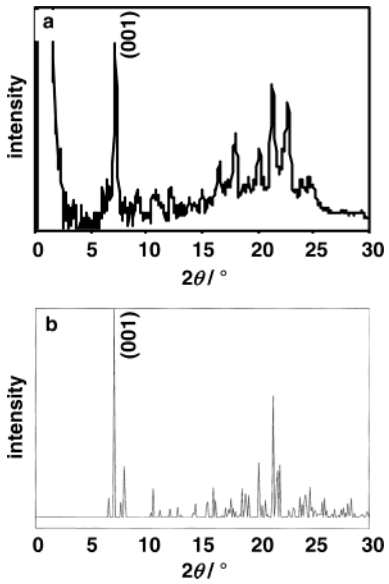

FIGURE 8. Powder X-ray diffraction diagrams of **2b**: (a) the xerogel prepared from benzene and (b) theoretical profile illustrated using the X-ray crystallographic data.

in a thermostated oil bath. The temperature was raised at a rate of 3 °C min^{-1}. Here, the T_{gel} was defined as the temperature at which the gel turned into the sol phase.

FTIR Measurement of Xerogels. All FTIR measurement of gels were performed in attenuated total reflection (ATR) mode. Xerogels were measured on the plate of universal ATR.

Crystal Structure Determinations. X-ray diffraction data were collected on a diffractometer with a 2D area detector using graphite-monochromatized Cu K radiation ($\lambda = 1.5418$). Lattice parameters were obtained by least-squares analysis from reflections for three oscillation images. Direct methods (SIR92) were used for the structure solution. All calculations were performed using on the TEXSAN[17] or Crystal Structure[18] crystallographic software package. For **2b**, the structure was refined by the full matrix least-squares procedure using observed reflections ($>2.0\sigma$(I)) based on F^2. All non-hydrogen atoms were refined with anisotropic displacement parameters, and hydrogen atoms were placed in idealized positions with isotropic displacement parameters relative to the connected non-hydrogen atoms and not refined. However, for **3b**, the low single crystallinity and small size made it difficult to determine electron density for one of the four *n*-butyl groups of the porphyrin and some solvated molecules. As a result, only a limited number of the atoms around the porphyrin ring were refined with anisotropic displacement parameters by the full matrix least-squares procedure using observed reflections ($>2.0\sigma$(I)) based on F^2, and hydrogen atoms were placed in idealized positions with isotropic displacement parameters relative to the connected non-hydrogen atoms and not refined. The relative high *R*-value is due to disorders of the butyl group

(17) TEXSAN, X-ray structure analysis package; Molecular Structure Corporation, The Woodlands, TX, 1985.
(18) Crystal Structure, X-ray structure analysis package; Molecular Structure Corporation.

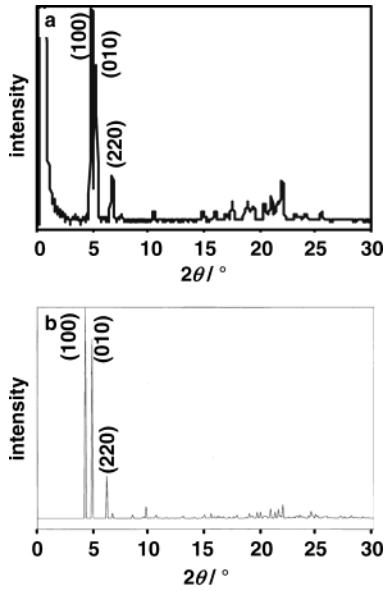

FIGURE 9. Powder X-ray diffraction diagrams of **3b**: (a) the xerogel prepared from benzene and (b) theoretical profile illustrated using the X-ray crystallographic data.

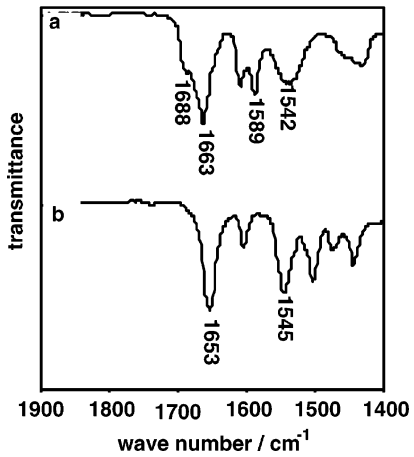

FIGURE 10. FTIR spectra of (a) **2b** and (b) **3b** xerogels prepared from benzene.

TABLE 3. FTIR Spectroscopic Absorption Bands (cm^{-1}) Data for Xerogels Obtained from 2a, 3a, 4a, 2b, and 3b[a]

compound	amide I	amide II
2a	1681/1650	1587/1557
3a	1649	1547
4a	several peaks	several peaks
2b	1688/1663	1589/1542
3b	1653	1545

[a] The xerogels of **2a**, **3a**, and **4a** were obtained from cyclohexane gel (25.0 g dm^{-3}), and those of **2b**, and **3b** were from benzene gel (25.0 g dm^{-3}).

and the solvated molecules. Crystallographic parameters are summarized in Table 2.

Powder X-ray Diffraction. The gel was prepared in a sample tube and frozen by liquid nitrogen. The frozen specimen was evaporated by a vacuum pump for 1 day. The obtained xerogel was put into a glass capillary tube ($\Phi = 0.3$ mm). X-ray diffractograme was recorded on an imaging plate using Cu radiation ($\lambda = 1.54178$ Å at a distance of 15 cm).

SEM Observations. The gel was prepared in a sample tube and frozen by liquid nitrogen. The frozen specimen was evaporated by a vacuum pump for 1 day. The obtained xerogel was shielded with platin. The accelerating voltage of SEM was 25.0 kV, and the emission current was 10 μA.

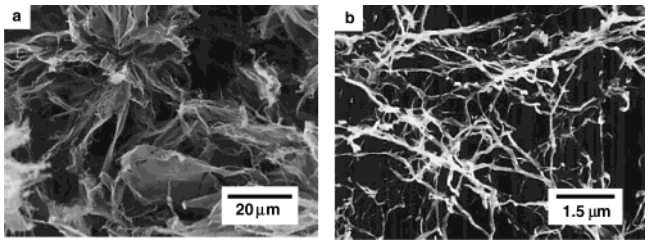

FIGURE 11. SEM images of (a) **2a** and (b) **3a** xerogels prepared from cyclohexane.

Materials. 5,10,15,20-Tetrakis(3′,5′-dihydroxyphenyl)porphine, 5,10,15,20-tetrakis(4′-hydroxyphenyl)porphine, and 5,10,15,20-tetrakis(3′-hydroxyphenyl)porphine were obtained from 5,10,15,20-tetrakis(3′,5′-dimethoxyphenyl)porphine, 5,10,15,20-tetrakis(4′-methoxyphenyl)porphine, and 5,10,15,20-tetrakis(3′-methoxyphenyl)porphine, respectively, which were synthesized by Adler method.[19] The demethylation reactions were carried out with boron tribromide to give 5,10,15,20-tetrakis(3′,5′-dihydroxyphenyl)porphine, 5,10,15,20-tetrakis(4′-hydroxyphenyl)porphine, and 5,10,15,20-tetrakis(3′-hydroxyphenyl)porphine in satisfactory yields. *N*-Dodecylbromoacetamide and *N*-butylbromoacetamide[20] were prepared by Schotten−Baumann reaction from bromoacetyl chloride with dodecylamine or butylamine, respectively.

5,10,15,20-Tetrakis[3′,5′-bis(*N*-dodecylamidemethoxy)phenyl]porphine (2a). A mixture of 5,10,15,20-tetrakis(3′,5′-dihydroxyphenyl)porphine (300 mg, 0.40 mmol), *N*-dodecylbromoacetamide (1.98 g, 6.46 mmol), and well-pulverized K_2CO_3 (843 mg, 6.46 mmol) in 20 mL of dry DMF was warmed at 60 °C for 2 days. The solvent was evaporated under reduced pressure, and the residue was extracted with chloroform. The organic layer was washed with 0.01 M hydrochloric acid, aqueous 5% $NaHCO_3$, and water and then was dried over Na_2SO_4. After the solvent was evaporated under reduced pressure, the solid residue was further purified through chromatography [silica gel, $CHCl_3$/MeOH = 100:1 (v/v)] to give **2a** in 42% (438 mg): mp 168−169 °C; ^{1}H NMR (600 MHz, $CDCl_3$, TMS, rt) δ −2.88 (s, 2H), 0.83 (t, $J = 7.1$, 24H), 1.19−1.58 (m, 144H), 1.58 (m, 2H), 3.38 (q, $J = 6.8$, 16H), 4.68 (s, 16H), 6.68 (t, $J = 5.9$, 8H), 6.97 (s, 4H), 7.50 (s, 8H), 8.86 (s, 8H); MALDI-TOF-MS [dithranol] *m*/*z* calcd 2546.7, found 2546.2; IR (ATR) 3317, 2924, 2854, 1663, 1595 cm^{-1}. Anal. Calcd for $C_{156}H_{246}N_{12}O_{16}$·2.0$H_2O$: C, 72.57; H, 9.76; N, 6.51. Found: C, 72.54; H, 9.62; N, 6.37.

5,10,15,20-Tetrakis(4′-*N*-dodecylamidemethoxyphenyl)porphine (3a). Compound **3a** was obtained as a purple solid in 26% yield by a method similar to the synthesis of compound **2a** from 5,10,15,20-tetrakis(4′-hydroxyphenyl)porphine and *N*-dodecylbromoacetamide: mp 197−198 °C; ^{1}H NMR (600 MHz, $CDCl_3$, TMS, rt) δ −2.78 (s, 2H), 0.84 (t, $J = 7.1$, 12H), 1.22−1.43 (m, 72H), 1.68 (m, 2H), 3.49 (q, $J = 6.7$, 8H), 4.79 (s, 8H), 6.81 (t, $J = 5.4$, 8H), 7.32 (d, $J = 8.3$, 8H), 8.16 (d, $J = 8.2$, 8H), 8.82 (s, 8H); MALDI-TOF-MS [dithranol] *m*/*z* calcd 1581.2, found 1581.6; IR (ATR) 3318, 2924, 2858, 1664, 1536 cm^{-1}. Anal. Calcd for $C_{100}H_{138}N_8O_8$·1.0 H_2O: C, 75.15; H, 8.83; N, 7.01. Found: C, 75.13; H, 8.78; N, 7.06.

5,10,15,20-Tetrakis(3′-*N*-dodecylamidemethoxyphenyl)porphine (4a). Compound **4a** was obtained as a purple solid in 20% yield by a method similar to the synthesis of compound **2a** from 5,10,15,20-tetrakis(3′-hydroxyphenyl)porphine and *N*-dodecylbromoacetamide: mp 165−166 °C; ^{1}H NMR (250 MHz, $CDCl_3$, TMS, rt) δ −2.82 (s, 2H), 0.83 (t, 12H), 1.18 (m,

(19) Adler, A. D. *J. Org. Chem.* **1967**, *32*, 476.
(20) (a) Schotten, C. *Ber.* **1884**, *17*, 2554. (b) Baumann, E. *Ber.* **1886**, *19*, 3218.

80H), 3.36 (q, 8H), 4.71 (s, 8H), 6.72 (t, 4H), 7.37 (d, 4H), 7.70 (t, 4H), 7.82 (s, 4H), 7.90 (d, 4H), 8.85 (s, 8H); MALDI-TOF-MS [dithranol] *m*/*z* calcd 1581.2, found 1580.4; IR (ATR) 3317, 2923, 2853, 1662, 1538 cm^{-1}. Anal. Calcd for $C_{100}H_{138}N_8O_8 \cdot 1.5\ H_2O$: C, 74.73; H, 8.84; N, 6.97. Found: C, 74.84; H, 8.69; N, 6.81.

5,10,15,20-Tetrakis[3′,5′-bis(*N*-butylamidemethoxy)-phenyl]porphine (2b). Compound **2b** was obtained as a purple solid in 46% yield by a method similar to the synthesis of compound **2a** from 5,10,15,20-tetrakis(3′,5′-hydroxyphenyl)-porphine and *N*-butylbromoacetamide: mp 194−195 °C; ^{1}H NMR (250 MHz, $CDCl_3$, TMS, rt) δ −2.88 (s, 2H), 0.91 (t, J = 7.2, 24H), 1.29 (m, 16H), 1.51 (m, 16H), 3.35 (q, J = 6.7, 16H), 4.67 (s, 16H), 6.76 (t, J = 5.8, 8H), 6.97 (s, 4H), 7.49 (s, 8H), 8.86 (s, 8H); MALDI-TOF-MS [dithranol] *m*/*z* calcd 1649.0, found 1648.9; IR (ATR) 3318, 2930, 1663, 1588, 1172 cm^{-1}. Anal. Calcd for $C_{92}H_{118}N_{12}O_{16}$: C, 67.05; H, 7.22; N, 10.20. Found: C, 66.92; H, 7.21; N, 10.14.

5,10,15,20-Tetrakis(4′-*N*-butylamidemethoxyphenyl)-porphine (3b). Compound **3b** was obtained as a purple solid in 61% yield by a method similar to the synthesis of compound **2a** from 5,10,15,20-tetrakis(4′-hydroxyphenyl)porphine and *N*-butylbromoacetamide: mp 254−255 °C; ^{1}H NMR (250 MHz, $CDCl_3$, TMS, rt) δ −2.79 (s, 2H), 0.98 (t, J = 7.2, 12H), 1.42 (m, 8H), 1.61 (m, 8H), 3.45 (q, J = 6.7, 8H), 4.80 (s, 8H), 6.81 (t, 8H), 7.30 (d, J = 8.6, 8H), 8.14 (d, J = 8.5, 8H), 8.83 (s, 8H); MALDI-TOF-MS [dithranol] *m*/*z* calcd 1132.4, found 1131.9; IR (ATR) 1653, 1545, 1239 cm^{-1}. Anal. Calcd for $C_{68}H_{74}N_8O_8 \cdot 0.5\ H_2O$: C, 71.62; H, 6.63; N, 9.83. Found: C, 71.35; H, 6.65; N, 9.71.

Supporting Information Available: ^{1}H NMR spectra of **2a**, **2b**, **3a**, **3b**, and **4a**. This material is available free of charge via the Internet at http://pubs.acs.org.

JO0341822